AIP | The Journal of Chemical Physics

Differential cross sections for electron impact excitation of the electronic bands of phenol

R. F. C. Neves, D. B. Jones, M. C. A. Lopes, K. L. Nixon, G. B. da Silva, H. V. Duque, E. M. de Oliveira, R. F. da Costa, M. T. do N. Varella, M. H. F. Bettega, M. A. P. Lima, K. Ratnavelu, G. García, and M. J. Brunger

Citation: The Journal of Chemical Physics **142**, 104305 (2015); doi: 10.1063/1.4913825
View online: http://dx.doi.org/10.1063/1.4913825
View Table of Contents: http://scitation.aip.org/content/aip/journal/jcp/142/10?ver=pdfcov
Published by the AIP Publishing

Differential cross sections for electron impact excitation of the electronic bands of phenol

R. F. C. Neves,[1,2,3] D. B. Jones,[1] M. C. A. Lopes,[3] K. L. Nixon,[3] G. B. da Silva,[1,4] H. V. Duque,[1,3] E. M. de Oliveira,[5] R. F. da Costa,[6] M. T. do N. Varella,[7] M. H. F. Bettega,[8] M. A. P. Lima,[5] K. Ratnavelu,[9] G. García,[10] and M. J. Brunger[1,9,a)]

[1]*School of Chemical and Physical Sciences, Flinders University, GPO Box 2100, Adelaide SA 5001, Australia*
[2]*Instituto Federal do Sul de Minas Gerais, Campus Poços de Caldas, Minas Gerais, Brazil*
[3]*Departamento de Física, UFJF, Juiz de Fora, Minas Gerais, Brazil*
[4]*Universidade Federal de Mato Grosso, Barra do Garças, Mato Grosso, Brazil*
[5]*Instituto de Física "Gleb Wataghin," Universidade Estadual de Campinas, 13083-859 Campinas, São Paulo, Brazil*
[6]*Centro de Ciências Naturais e Humanas, Universidade Federal do ABC, 09210-580 Santo André, São Paulo, Brazil*
[7]*Instituto de Física, Universidade de São Paulo, CP 66318, 05315-970 São Paulo, Brazil*
[8]*Departamento de Física, Universidade Federal do Paraná, CP 19044, 81531-990 Curitiba, Paraná, Brazil*
[9]*Institute of Mathematical Sciences, University of Malaya, 50603 Kuala Lumpur, Malaysia*
[10]*Instituto de Física Fundamental, CSIC, Madrid E-28006, Spain*

(Received 23 December 2014; accepted 25 January 2015; published online 10 March 2015)

We report results from a joint theoretical and experimental investigation into electron scattering from the important organic species phenol (C_6H_5OH). Specifically, differential cross sections (DCSs) have been measured and calculated for the electron-impact excitation of the electronic states of C_6H_5OH. The measurements were carried out at energies in the range 15–40 eV, and for scattered-electron angles between 10° and 90°. The energy resolution of those experiments was typically ~80 meV. Corresponding Schwinger multichannel method with pseudo-potentials calculations, with and without Born-closure, were also performed for a sub-set of the excited electronic-states that were accessed in the measurements. Those calculations were conducted at the static exchange plus polarisation (SEP)-level using a minimum orbital basis for single configuration interaction (MOBSCI) approach. Agreement between the measured and calculated DCSs was typically fair, although to obtain quantitative accord, the theory would need to incorporate even more channels into the MOBSCI. [http://dx.doi.org/10.1063/1.4913825]

I. INTRODUCTION

Phenol is an important industrial aromatic compound and is considered to be a commodity chemical. It was originally isolated from coal tar but is now produced worldwide on a very large scale (in excess of ~7 × 10^9 kg/yr). The most modern method of production involves the partial oxidation of isopropyl benzene (via the Hock rearrangement), which also gives acetone as a secondary product.[1] Phenol is an important feedstock for the polymer industry, being a key starting material for polymers such as bakelite, polycarbonates, polyepoxides, and nylon. Phenol is also used in the preparation of the phenoxy herbicides and numerous pharmaceuticals.

We recently outlined our specific interest in electron–phenol scattering,[2–4] in terms of its relevance to understanding the treatment of biomass by atmospheric pressure plasmas.[5,6] In that application, free electrons or radicals generated within the plasma have the capability to overcome the natural resilience of biomass to degradation.[7] Specifically, lignocellulose may be broken-down via electron impact to yield fermentable sugars, which is important for intensifying the enzymatic hydrolysis process in view of improving bio-ethanol outputs. Phenol (C_6H_5OH) has been identified[8] as a potential target of electron-induced breakdown of lignin (a phenolic-based moiety), and so it represents an excellent prototype sub-unit for lignin. To gain a comprehensive understanding for the utility of atmospheric plasmas to economically generate bio-fuels and other useful industrial chemicals, plasma simulations are required. Those simulations, in turn, require complete sets of electron-impact gas phase cross sections from the prototypical molecules, such as phenol, relevant to the application in question. In this respect, we have already reported results from a detailed study into the excited electronic-state spectroscopy of phenol,[2] experimental and theoretical triple differential cross sections (DCSs) for electron-impact ionisation of phenol,[3] and most recently a study about the influence of electronic multichannel coupling on elastic electron–phenol scattering.[4] Here, we extend those earlier investigations by reporting experimental and theoretical differential cross sections for excitation of excited electronic-states in phenol, with our calculations being performed within a Schwinger Multichannel Method with Pseudo-potentials (SMCPP) framework.

Irrespective of our aim to provide reliable cross section data for plasma simulation studies, phenol possesses several intrinsic physico-chemical properties which, from our

a)Author to whom correspondence should be addressed. Electronic mail: Michael.Brunger@flinders.edu.au

experience with other scattering systems,[9–15] are anticipated to play important roles in the collision dynamics. Specifically, phenol has a permanent dipole moment of magnitude ~1.33 D[16]–1.42 D[8] and a significant average dipole polarisability of 10.53 Å^3 Ref. 8 or 10.54 Å^3.[16] We, therefore, also sought to investigate how those physico-chemical properties manifested themselves in the behaviour of the electronic-state DCSs of phenol, with particular interest in analysing their influence on the angular distributions. In addition, in our earlier investigation of elastic scattering,[4] we found that the phenol and benzene DCSs were very similar, in terms of both their magnitude and angular distributions, at each energy studied in the 15–40 eV energy range. We, therefore, also wished to verify if such behaviour was maintained between phenol and benzene,[17] when comparing their corresponding electronic-state DCSs. Here, a link between phenol and benzene excited state transitions has previously been established.[2]

In addition to the previous results of our team on the scattering of electrons from phenol,[2–4,8] little other relevant work appears to be currently available in the literature. In this respect, we mention an earlier electron energy loss spectrum (EELS) at an incident electron energy (E_0) of 70 eV and at the scattered electron angle (θ) of 0°,[18] an electron transmission study of the negative ion states of phenol from Jordan *et al.*,[19] a dissociative electron attachment investigation[20] and a photo-absorption spectrum.[21] Given the long-term importance of phenol in organic chemistry (and other areas of chemistry), this sparsity of data is a little surprising but as a consequence we believe the present theoretical and experimental efforts are original.

The structure of this paper is as follows. In Sec. II, we describe our experimental methods and analysis procedures, while in Sec. III, details of our present computations can be found. Thereafter, in Sec. IV, our experimental and SMCPP DCSs are presented and discussed, before some conclusions from this study are given.

II. EXPERIMENTAL METHODS AND ANALYSIS

To derive absolute differential cross sections for electron impact excitation of the bands of inelastic electronic-states[2] in phenol, we begin with measurements of EELSs. A typical example for some of the EELS measured in this investigation is given in Fig. 1, which also indicates the bands of electronic-states of phenol, below the first ionisation threshold, as classified in Jones *et al.*[2] The present energy loss spectra were collected by an apparatus based at Flinders University, as originally described in Brunger and Teubner.[22] However, to ensure this paper is self-contained, we note that in this work, a monochromated electron beam with energies in the range 15–40 eV and with a typical current of 1–5 nA was incident on an orthogonal beam of phenol molecules. That molecular beam was formed by gently heating a phenol sample to $T \sim 35$–45 °C and allowing the vapour from that sample to enter the collision region through a 0.7 mm internal diameter single capillary. Here, the vapour pressure was regulated using a variable leak-valve. Note that the phenol sample (GPR-BOH; >99% assay) had been degassed through repeated freeze-pump-thaw

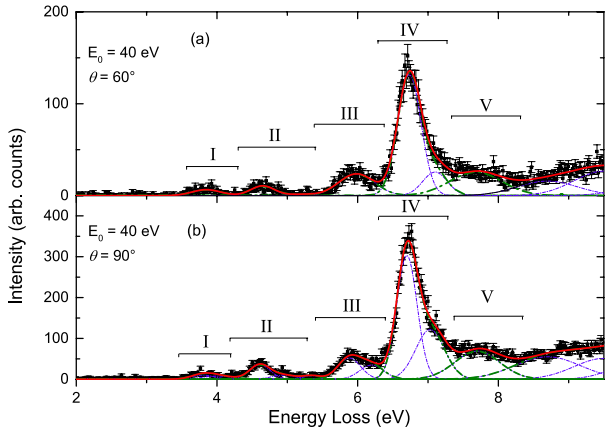

FIG. 1. Typical electron energy loss spectrum of phenol at (a) $E_0 = 40$ eV and $\theta = 60°$ and (b) $E_0 = 40$ eV and $\theta = 90°$. The overall spectral deconvolution fit is denoted by the solid red line, while the fits to the various bands are also shown by the dashed lines. The short-dashed blue lines represent the individual Gaussians employed in the fit, while the long-dashed green lines indicate the fits for each respective band I–V. See Ref. 2 for further details. Note that in each case, the elastic peak has been suppressed for clarity.

cycles. Further note that to facilitate a stable phenol beam, the gas handling lines and vacuum chamber were heated to at most 65 °C. Under the stable beam conditions maintained during the EELS measurements, the phenol vacuum chamber pressure was always kept below 5×10^{-6} Torr to ensure that multiple scattering effects could be neglected. In the current study, the overall instrumental energy resolution was typically ~80 meV full-width at half-maximum (FWHM), while the scattered electron angle range was 10°–90°. EELS's were collected at each θ and incident electron energy (15, 20, 30, and 40 eV) by recording the number of scattered electrons detected at each energy loss value. The true electron count rate at each given energy loss was recorded using a multichannel scaler synchronised to a linear voltage ramp that varied the detected energy loss between −0.2 and 9.5 eV. In this way, a given EELS is built up by continually scanning over the selected range of energy loss values, so that the effect of any variations in the incident electron current or target beam flux is minimised. In general, at each E_0 and θ, the EELSs were measured 2–4 times to ensure that the measured inelastic to elastic ratios (see later) were reproducible.

In Jones *et al.*,[2] we previously outlined the electronic-state spectroscopy of phenol and thus the basis of our spectral deconvolution approach. We, therefore, do not repeat that detail here. Rather, we simply note that the various EELSs were deconvoluted, using a standard least-squares fitting procedure, into contributions arising from each individual or unresolved combination of excited electronic-states. Either one or two Gaussian functions were employed to describe the spectral profiles for each resolvable inelastic feature (band) and the elastic scattering peak, with the positions and widths of the Gaussians being guided by the results of the quantum chemistry calculations in Jones *et al.*[2] (see their Table 1) and our experimental energy resolution. The detailed quantum chemistry calculations[2] lead us to believe that Band I (see Fig. 1), over the energy loss (E_L) range ~3.4–4.3 eV, is comprised of two experimentally unresolved electronic states of triplet character. Band II (see

Fig. 1), over the E_L range ~4.3–5.4 eV, consists of a number of singlet and triplet states, including a weak dipole-allowed $\pi\pi^*$ transition. As noted in Jones *et al.*,[2] the states in Band II have attracted some interest as the observed dipole allowed $^1A'$ ($\pi\pi^*$) transition couples to the weakly dipole-allowed $^1A''$ ($\pi\sigma^*$) state through a conical intersection. The $^1A''$ state proceeds to photodissociate along an OH reaction coordinate owing to the antibonding character of the OH bond (see, for example, Refs. 23 and 24). The characterisation of electron-impact excitation of this band is thus crucial in assessing the potential of electron-driven degradation of phenolic species, such as lignin. Band III in the E_L ~ 5.4–6.3 eV (again, see Fig. 1) range is also dominated by dipole-allowed excitations, although some triplet contribution cannot be discounted. The spectroscopy of this band is also interesting as its behaviour is consistent with the $^1B_{1u}$ + $^3E_{2g}$ electronic-states in benzene.[17] We will return to this point later in Sec. IV. In the E_L ~ 6.3–7.3 eV energy loss range, labelled as Band IV (see Fig. 1), excitations have been assigned[2] to a rich mixture of dipole-allowed (singlet) and dipole-forbidden (triplet) states. Nonetheless, the spectroscopy is expected to be dominated by the strong $\pi\pi^*$ transitions associated with the aromatic ring. Here, again we can find a strong correlation with the excitation of the $^1E_{1u}$ benzene electronic-state (see Sec. IV).[17] Finally, significant experimental intensity can be found in Fig. 1 in the E_L ~ 7.3–8.3 eV range (Band V). That intensity has been ascribed[2] to a large number of Rydberg-like excitation processes up to the first ionization potential (8.64 eV[25]) in phenol. Full details of all our assignments can be found in Jones *et al.*[2] The amplitudes of the Gaussian functions were now varied in a least-squares fitting procedure to provide the best fit to the measured spectra (see Fig. 1). The ratio (R) of the area under the fitting function for each ith inelastic band to that under the elastic feature, at each E_0 and θ, is simply related to the ratio of the differential cross sections

$$R_i(E_0,\theta) = \frac{\sigma_i(E_0,\theta)}{\sigma_0(E_0,\theta)}. \quad (1)$$

Note that Eq. (1) is only valid if the transmission efficiency of the analyser remains constant over the energy loss and angular range studied, or is at least well characterised. Following an approach similar to that of Allan,[26] an additional focusing lens (synchronised to the voltage ramp) was also employed to minimise variations in the angular transmission efficiency for electrons detected with different energy losses. Our results suggest that the efficiency is unity, to within an uncertainty of 20%. The results for the present measured R_i, for each of Bands I–V, are given, at each energy, in the first columns of Tables I–V, respectively.

It follows from Eq. (1) that the product of $R_i \times \sigma_0$ then gives the required electronic-state band differential cross section provided the elastic DCS, σ_0, is known. In this investigation, we have utilised the benzene elastic DCS from Cho *et al.*[27] and Gulley and Buckman[28] to place our inelastic data, at each E_0 and θ, onto an absolute scale. The efficacy and accuracy of such a choice was recently addressed in detail by da Costa *et al.*,[4] and so we do not repeat that argument here. Suffice it to say, that at each energy, the phenol elastic SMCPP differential cross sections were generally found to be in very good agreement with the corresponding elastic benzene measurements of Cho *et al.*,[27] in terms of both their shapes and absolute values, due to its more exact incorporation for multichannel coupling effects[4] than was previously possible. Thus, we could have equally well used the elastic phenol SMCPP results of da Costa *et al.*[4] to effect the normalisation in this case. Note that where agreement between the benzene data and the elastic SMCPP calculation for phenol is perhaps worst (e.g., at 40 eV and 90°), the difference ~28% is of the same order of magnitude as the uncertainties we quote in Tables I–V on our electronic-state DCS of Bands I–V. Hence the choice of normalisation is not critical in this case. This level of agreement between phenol and benzene, in the elastic channel, over such an energy range, is intriguing given that benzene is non-polar while phenol has a permanent dipole moment (although both molecules do have large and almost identical dipole polarisibilities). However as the magnitude of the dipole moment in phenol is only ~2/3 that of water, we would anticipate that the polarisability and short-range correlations would be more important in describing the scattering dynamics in phenol thus giving a plausible rationale for the behaviour observed in the elastic channel. We will return to this point in Sec. IV, where we compare the present 15 eV and 30 eV Band III and Band IV DCSs with those for the ($^1B_{1u}$ + $^3E_{2g}$) and $^1E_{1u}$ electronic-states of benzene, respectively. The results of the present inelastic DCSs, and their associated uncertainties, are listed in Tables I–V for the

TABLE I. Present experimental electronic-to-elastic ratios (×10^{-3}), differential cross sections (×10^{-23} m^2/sr), and related uncertainty (%) for electron-impact excitation of the first electronic band (Band I: E_L = 3.4–4.3 eV) in phenol.

	15 eV			20 eV			30 eV			40 eV		
θ (deg)	Ratio	DCS	Uncertainty	Ratio	DCS	Uncertainty	Ratio	DCS	Uncertainty	Ratio	DCS	Uncertainty
10	…	…	…	0.09	12.83	57	0.12	8.54	71	…	…	…
15	…	…	…	0.36	12.65	66	0.14	4.64	97	0.31	8.09	88
20	0.92	24.96	43	0.25	4.60	67	0.18	2.54	81	0.40	3.66	74
30	8.08	63.16	42	2.11	9.25	44	1.46	3.63	70	2.20	3.51	75
40	14.19	27.29	46	3.83	4.23	57	2.57	2.65	63	2.74	2.62	74
50	34.39	30.40	28	3.71	2.46	67	2.73	2.45	37	2.27	2.10	61
60	19.80	17.22	44	4.84	4.00	43	2.66	2.21	49	3.59	2.17	59
70	17.10	17.93	38	6.62	5.97	34	4.74	2.95	42	5.12	1.94	36
80	19.84	23.71	31	11.00	9.17	51	5.83	2.79	40	4.62	1.55	45
90	31.64	37.52	35	11.44	8.18	41	5.25	2.26	40	4.53	1.67	55

TABLE II. Present experimental electronic-to-elastic ratios ($\times 10^{-3}$), differential cross sections ($\times 10^{-23}$ m^2/sr), and related uncertainty (%) for electron-impact excitation of the second electronic band (Band II: $E_L = 4.3$–5.4 eV) in phenol.

	15 eV			20 eV			30 eV			40 eV		
θ (deg)	Ratio	DCS	Uncertainty	Ratio	DCS	Uncertainty	Ratio	DCS	Uncertainty	Ratio	DCS	Uncertainty
10	...	...	...	1.09	149.62	31	2.63	184.00	28	2.12	149.17	31
15	...	...	...	3.68	128.13	30	1.38	45.31	37	1.01	26.67	51
20	4.38	118.43	33	2.03	37.46	32	1.65	23.49	29	1.92	17.81	41
30	22.61	176.79	30	8.77	38.49	27	7.13	17.75	30	10.76	17.15	35
40	34.99	67.32	30	14.34	15.81	30	10.83	11.16	31	8.34	7.97	54
50	87.83	77.64	24	16.41	10.91	31	6.49	5.81	26	4.27	3.96	43
60	73.96	64.35	32	12.80	10.57	30	4.69	3.89	29	4.98	3.00	41
70	48.70	51.09	24	16.32	14.73	30	7.81	4.86	33	8.92	3.38	29
80	60.86	72.73	25	28.43	23.71	54	9.63	4.60	29	9.20	3.09	31
90	51.00	60.49	36	29.43	21.04	42	10.89	4.69	29	10.87	4.00	35

electron impact excited Bands I–V of phenol electronic-states, respectively. These data are also plotted in Figs. 2–6.

Finally, we have paid some attention to the identification and quantification of all possible sources of experimental error in this study. Here, our error analysis combines in quadrature the statistical uncertainty associated with the deconvolution of our energy loss spectra, the uncertainty relating to the transmission efficiency of our analyser and the uncertainty on the absolute elastic scattering data. The overall DCS uncertainties on our inelastic phenol DCS are found to be in the range 22%–97% with the precise error depending on the energy, scattering angle, and electronic-state band in question. Note that the upper limit on this error range is only for the Band I triplet states at forward scattering angles, while the vast majority of the present measured DCS has errors in the 22%–35% range.

III. THE SMCPP

The Schwinger multichannel method (SMC)[29] is a well established approach to obtain the scattering amplitude for collisions of low-energy electrons with molecules. It is an *ab-initio* method that includes important effects such as exchange, polarisation, and electronic multichannel coupling. For this application of the method, we have used the parallel version[30] of the SMC implementation that employs norm-conserving pseudo-potentials[31] (SMCPP) and single-excitation configuration interaction techniques for the target description.[32] Here, we give the working expression for the scattering amplitude,

$$f(\mathbf{k}_f, \mathbf{k}_i) = -\frac{1}{2\pi} \sum_{m,n} \langle S_{\mathbf{k}_f} | V | \chi_m \rangle (d^{-1})_{mn} \langle \chi_n | V | S_{\mathbf{k}_i} \rangle, \tag{2}$$

where

$$d_{mn} = \langle \chi_m | \left[\frac{\hat{H}}{N+1} - \frac{\hat{H}P + P\hat{H}}{2} + \frac{PV + VP}{2} - VG_P^{(+)}V \right] | \chi_n \rangle. \tag{3}$$

In the expressions above, P is a projector onto N_{open} energy-allowed target electronic channels, i.e.,

$$P = \sum_{\ell=1}^{N_{open}} | \Phi_\ell \rangle \langle \Phi_\ell | . \tag{4}$$

In addition, $G_P^{(+)}$ is the free-particle Green's function projected onto the P space, V is the projectile-target interaction potential, $\mathbf{k}_i$ ($\mathbf{k}_f$) is the incoming (outgoing) projectile wave vector, and $\hat{H} = E - H$ is the total energy (ground state energy plus kinetic energy of the incoming electron) minus the Hamiltonian of the $(N + 1)$-electron system under the field of fixed nuclei. The

TABLE III. Present experimental electronic-to-elastic ratios ($\times 10^{-3}$), differential cross sections ($\times 10^{-23}$ m^2/sr), and related uncertainty (%) for electron-impact excitation of the third electronic band (Band III: $E_L = 5.4$–6.3 eV) in phenol.

	15 eV			20 eV			30 eV			40 eV		
θ (deg)	Ratio	DCS	Uncertainty	Ratio	DCS	Uncertainty	Ratio	DCS	Uncertainty	Ratio	DCS	Uncertainty
10	...	...	...	2.28	311.01	33	8.54	596.30	24	8.21	577.41	24
15	...	...	...	7.38	257.00	23	5.01	164.23	26	5.41	142.43	27
20	10.48	283.18	33	6.04	111.43	23	5.73	81.77	23	9.63	89.28	25
30	46.64	364.61	31	14.16	62.15	24	18.12	45.08	26	23.11	36.83	24
40	59.33	114.14	26	33.66	37.13	24	23.56	24.29	23	20.76	19.85	37
50	122.05	107.89	23	31.82	21.16	28	16.52	14.80	23	13.36	12.37	25
60	83.91	73.00	28	25.08	20.72	28	14.41	11.95	25	14.76	8.90	26
70	76.56	80.31	22	28.51	25.74	23	17.56	10.92	27	17.82	6.75	25
80	90.43	108.07	25	37.71	31.45	38	24.01	11.48	24	20.65	6.94	25
90	58.85	69.79	27	44.73	31.98	35	22.04	9.50	28	21.20	7.80	26

TABLE IV. Present experimental electronic-to-elastic ratios ($\times 10^{-3}$), differential cross sections ($\times 10^{-23}$ m^2/sr), and related uncertainty (%) for electron-impact excitation of the fourth electronic band (Band IV: $E_L = 6.3$–7.3 eV) in phenol.

	15 eV			20 eV			30 eV			40 eV		
θ (deg)	Ratio	DCS	Uncertainty	Ratio	DCS	Uncertainty	Ratio	DCS	Uncertainty	Ratio	DCS	Uncertainty
10	…	…	…	8.14	1112.31	38	46.99	3281.87	23	46.35	3261.67	22
15	…	…	…	27.83	968.99	22	24.93	816.65	24	28.95	762.30	24
20	35.25	952.30	37	21.96	405.41	22	25.11	358.15	22	43.51	403.25	22
30	116.61	911.63	38	41.27	181.16	23	79.95	198.92	22	101.73	162.15	22
40	95.78	184.28	35	129.03	142.32	22	124.71	128.58	22	96.28	92.04	23
50	227.35	200.98	23	133.57	88.83	22	75.46	67.61	23	59.10	54.72	22
60	187.61	163.22	23	89.14	73.63	24	61.08	50.63	24	66.04	39.82	23
70	192.70	202.15	24	81.87	73.93	22	76.35	47.49	23	85.88	32.55	23
80	180.69	215.93	22	129.76	108.22	29	106.14	50.73	22	98.82	33.20	23
90	175.61	208.27	22	161.10	115.18	27	113.13	48.76	23	102.62	37.76	23

latter is given by $H = H_0 + V$, where H_0 describes the non-interacting electron-molecule system and $S_{\mathbf{k}}$ is a solution of H_0, namely, the product of a plane wave (projectile) and a target state Φ_ℓ (single configuration interaction description). For the expansion of the variational scattering wave function, the method employs trial basis sets comprising $(N+1)$-particle configuration state functions (CSFs) denoted by χ_m and built from spin-adapted, anti-symmetrized products of target electronic states and projectile scattering orbitals. The open electronic collision channels are included in the P space and the dynamical response of the target electrons to the projectile field (correlation-polarization effects) is accounted for through virtual excitations of the target. In this case, the CSFs are given by

$$|\chi_m\rangle = \mathcal{A}_{N+1}|\Phi_i(1,\ldots,N)\rangle \otimes |\varphi_j(N+1)\rangle, \qquad (5)$$

where for $i > 0$, $|\Phi_i\rangle \equiv {}^{(2S+1)}(h_i \rightarrow p_i)$ is a singly excited state obtained by promoting one electron from a hole orbital (h_i) of the ground state $\Phi_0(1,\ldots,N)$ to a particle orbital (p_i), with either singlet $(S = 0)$ or triplet $(S = 1)$ spin coupling, though only $(N+1)$-electron configurations with total spin $S = 1/2$ (doublets) are actually taken into account. If we have N_{open} states in Eq. (4), this level of calculation is denoted as an N_{open}-channel coupling scheme at the static-exchange-plus-polarization (acronym is N_{open}ch-sep) approximation. In order to transform the scattering amplitude from the body-fixed frame (the reference frame best suited for carrying out the calculations) to the laboratory-fixed frame (the reference frame where the z-axis is aligned with the direction of the incident wave vector, i.e., $\mathbf{k}_i = k_i\hat{\mathbf{z}}$), we expand $\mathbf{k}_f$ in partial waves,

$$f(\mathbf{k}_f,\mathbf{k}_i) \equiv \langle \mathbf{k}_f|f|\mathbf{k}_i\rangle = \sum_{\ell=0}^{\ell_{max}} \sum_{m=-\ell}^{\ell} \langle \mathbf{k}_f|\ell m\rangle f(\ell m,\mathbf{k}_i), \qquad (6)$$

where $\langle \mathbf{k}_f|\ell m\rangle$ is a spherical harmonic that can be easily converted from the body to the lab-frame and $f(\ell m,\mathbf{k}_i) = \langle \ell m|f|\mathbf{k}_i\rangle$ can be understood as the scattering amplitude of an electron entering the interaction region in a plane-wave $|\mathbf{k}_i\rangle$ and leaving it in a partial wave $|\ell m\rangle$. Cross sections obtained with $f(\ell m,\mathbf{k}_i)$ will be referred to by the acronym $L_{max}KL$, where K indicates that the incoming electron propagates in a plane-wave, L indicates that the outgoing electron propagates out in a partial wave, and L_{max} indicates the maximum value of L used in the calculation. As discussed in the accompanying elastic scattering and total cross section paper, all differential cross sections in this study over the entire energy range (5-50 eV) are numerically converged with $L_{max} = 10$ (except for 50 eV that demands $L_{max} = 13$), if combined with a quadrature point distribution, using a 26 Gauss-Legendre scheme for $0 \le \theta_i \le \pi$ and 52 points for $0 \le \phi_i \le 2\pi$ to describe $\mathbf{k}_i(\theta_i,\phi_i)$ in spherical coordinates. Another form of expressing

TABLE V. Present experimental electronic-to-elastic ratios ($\times 10^{-3}$), differential cross sections ($\times 10^{-23}$ m^2/sr), and related uncertainty (%) for electron-impact excitation of the Rydberg bands (Band V: $E_L = 7.3$–8.3 eV) in phenol.

	15 eV			20 eV			30 eV			40 eV		
θ (deg)	Ratio	DCS	Uncertainty	Ratio	DCS	Uncertainty	Ratio	DCS	Uncertainty	Ratio	DCS	Uncertainty
10	…	…	…	2.44	333.53	28	8.43	589.13	24	9.30	654.38	23
15	…	…	…	8.52	296.79	32	4.96	162.58	37	7.14	188.06	26
20	12.94	349.49	34	5.52	101.82	31	6.76	96.37	26	9.03	83.69	24
30	73.67	575.92	33	8.54	37.50	31	19.89	49.48	27	30.31	48.32	25
40	81.52	156.84	29	35.35	38.99	26	31.50	32.48	24	26.55	25.38	30
50	232.11	205.18	22	42.29	28.12	24	22.35	20.03	25	17.40	16.11	25
60	220.08	191.47	23	31.96	26.40	28	17.88	14.82	23	22.67	13.67	25
70	164.67	172.73	25	37.46	33.83	23	26.09	16.23	25	30.44	11.54	23
80	182.88	218.54	26	49.56	41.33	42	31.21	14.92	23	30.15	10.13	24
90	114.85	136.21	22	63.92	45.70	38	32.86	14.16	27	32.52	11.97	25

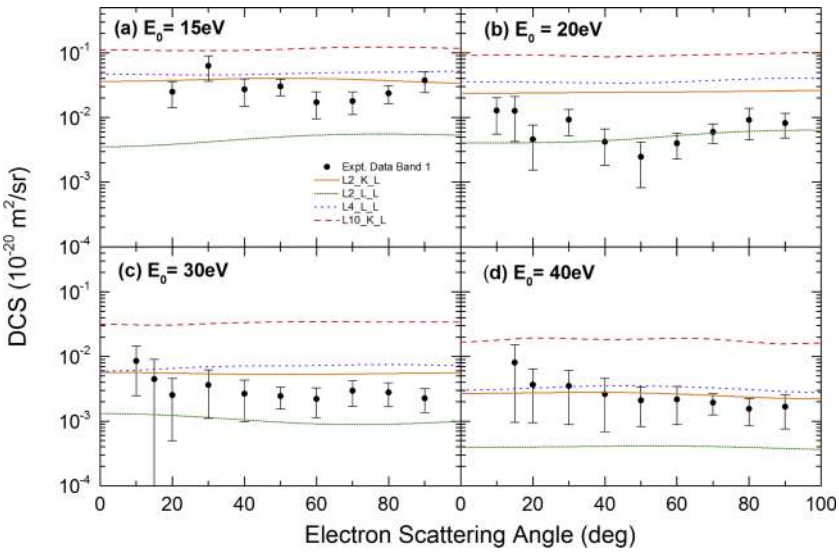

FIG. 2. Present differential cross sections ($\times 10^{-20}$ m^2/sr) for electron impact excitation of the Band I electronic states in phenol. Current measured data (•) and SMCPP-SEP calculations for 33 open channels at the L2KL level (orange line), L2LL level (green line), L4LL level (blue line), and L10KL level (red line) are shown (see also legend on figure). Note that L2KL denotes an electron entering in a plane wave and exiting in partial waves up to $L_{\max} = 2$; L2LL denotes an electron entering and exiting in partial waves up to $L_{\max} = 2$; L4LL is the same as L2LL but with $L_{\max} = 4$; while L10KL is the same as L2KL except now $L_{\max} = 10$.

the scattering amplitude is through the expansion of $\mathbf{k}_i$ in partial waves, so that now the DCSs are obtained from

$$\langle \mathbf{k}_f|f|\mathbf{k}_i\rangle = \sum_{l=0}^{\ell_{max}} \sum_{l'=0}^{\ell_{max}} \langle \mathbf{k}_f|\ell m\rangle f(\ell m, \ell' m')\langle \ell' m'|\mathbf{k}_i\rangle. \quad (7)$$

In this expression, $f(\ell m, \ell' m') = \langle \ell, m|f|\ell', m'\rangle$ means a scattering amplitude of an electron entering the interaction region in a partial wave $|\ell', m'\rangle$ and leaving it in a partial wave $|\ell, m\rangle$. The acronym for cross sections obtained with this expression is $L_{max}LL$, where LL indicates that the incoming and outgoing electron travels in terms of partial waves and L_{max} indicates the maximum value of L used for both partial waves in the calculation. Expansion up to $L_{max} = 4$ is a common limitation of other scattering computer codes[33] and, in order to allow future comparisons, we have included results calculated from Eq. (7) with this value. This approximation will be referred to as $L4LL$. For some cases (elastic and dipole allowed singlet transitions), a Born-closure (BC) scheme was used following the same strategy as in the accompanying paper.[4]

This closure is obtained from the expression

$$f_{\mathrm{LAB}}^{\mathrm{closure}}(\mathbf{k}_f, \mathbf{k}_i) = f_{\mathrm{LAB}}^{\mathrm{FBA}}(\mathbf{k}_f, \mathbf{k}_i) + \sum_{\ell=0}^{\ell_{max}} \sum_{m=-\ell}^{m=\ell} \Big(f_{\mathrm{LAB}}(\ell m, \mathbf{k}_i) - f_{\mathrm{LAB}}^{\mathrm{FBA}}(\ell m, \mathbf{k}_i) \Big) Y_{\ell m}^*(\mathbf{k}_f), \quad (8)$$

where $f_{\mathrm{LAB}}^{\mathrm{FBA}}$ is the amplitude for the permanent dipole moment potential for the elastic process or for the dipole transition potential for inelastic dipole allowed processes. Both are obtained in the first Born approximation, in a closed form in the lab-frame. The amplitude $f_{\mathrm{LAB}}(\ell m, \mathbf{k}_i)$ is just the $f(\ell m, \mathbf{k}_i)$ of Eqs. (6) or (7) transformed to this frame. The acronym for DCS obtained with Eq. (8), using Eqs. (6) and (7), is $BC - L_{max}KL$ and $BC - L_{max}LL$, respectively. For small molecules, it is a common belief that the cross sections for triplet excitations, which are caused by short range potentials (exchange), demand small values of L_{max} for convergence. For dipole allowed transitions, it is also common to truncate the *ab-initio* method at $L_{max} = 2$ and do the Born-closure beyond this value

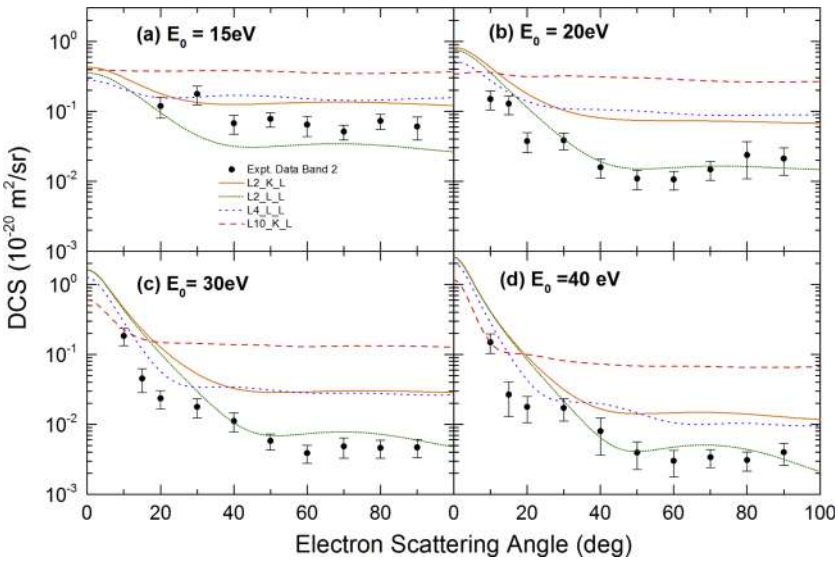

FIG. 3. Same as Fig. 2 but now for electron impact excitation of the Band II electronic states in phenol. Note that Born-closure has been incorporated to the singlet states within this band.

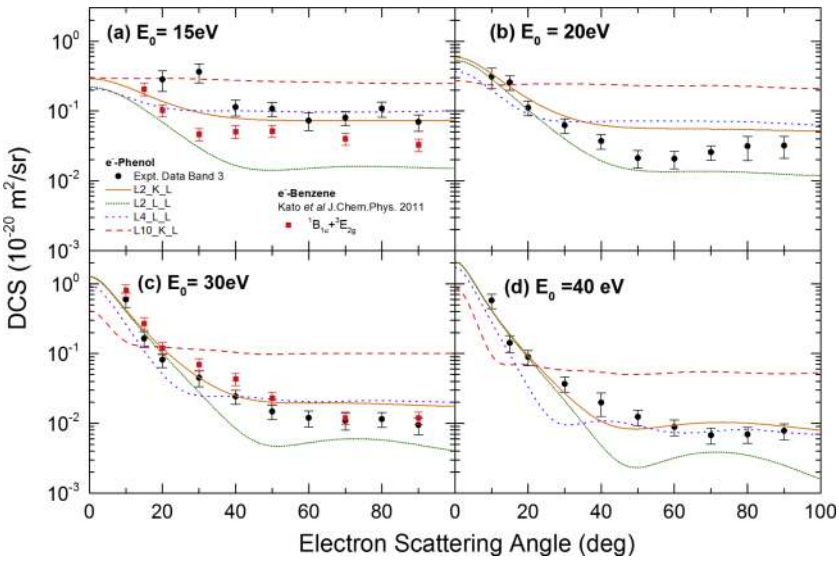

FIG. 4. Same as Fig. 2 but now for electron impact excitation of the Band III electronic states in phenol. Also shown are the earlier benzene data for excitation of the $(^1B_{1u} + {}^3E_{2g})$ electronic states from Kato *et al.*[17] (■). Note that Born-closure has been incorporated to the singlet states within this band.

(assuming that the dipole-transition should dominate the process). Although this low L_{max} behaviour was not seen even for triplets in the present application, we decided to report DCS obtained with $L_{max} = 2$ as well.

IV. RESULTS AND DISCUSSION

In Tables I–V, we present the current measured differential cross sections for electron-impact excitation of the Band I, Band II, Band III, Band IV, and Band V (see Fig. 1) electronic-states in phenol. Also shown in those tables are the associated overall errors on those DCSs, which are reported to the one standard deviation level. All these data are also plotted in Figs. 2–6, at each of 15 eV, 20 eV, 30 eV, and 40 eV impact electron energies. Additionally included in Figures 2–4 are the corresponding results from our calculations, at various levels of computational complexity. We now frame the remainder of our discussion by comparing, where possible, the present experimental and theoretical results for each Band in turn.

We have previously noted[2] that Band I consists of two triplet states (experimentally unresolved). Therefore, as the ground electronic state of phenol is a singlet state, we would anticipate that the electron exchange interaction would be the pre-dominant population mechanism for those triplet states. In Fig. 2, we find that at each energy investigated the angular distributions of the DCSs, for both the experiment, to within its uncertainties, and the various levels of theory are largely quasi-isotropic. This behaviour is perhaps not so surprising, as we had previously seen for the $X^1A_g \rightarrow \tilde{a}^3B_{1u}$ excitation in ethylene[34,35] a similar behaviour at intermediate energies such as in the present study. The various levels of theory presented in Fig. 2, all within our SMCPP-SEP approach and employing our minimum orbital basis for single configuration interaction (MOBSCI) strategy to represent the target, differ in respect to whether the electron enters the scattering region as a plane wave (K) or a spherical wave (L), up to some partial wave $L_{\max}$, and exits in a spherical wave again up to some value $L_{\max}$. Four different levels of results are presented, for Bands I, II, and III with L2KL denoting an electron entering in a plane wave

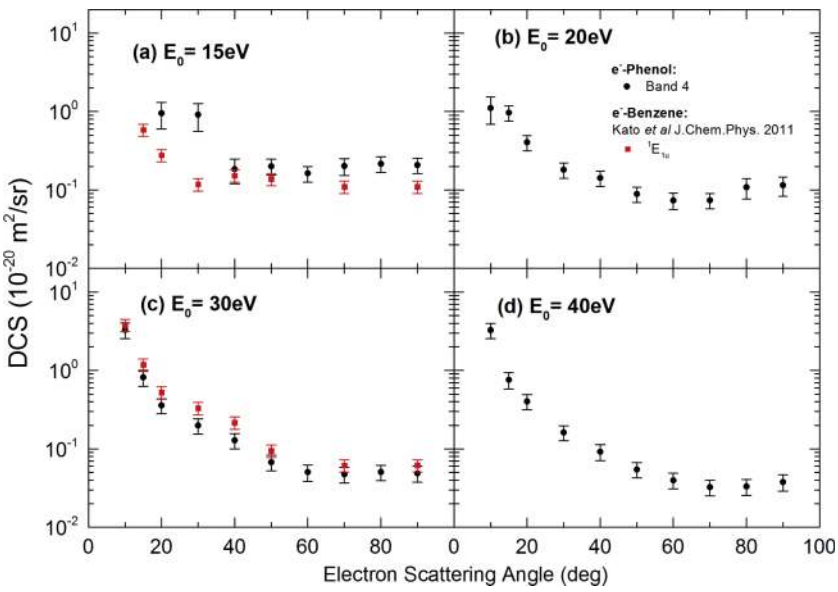

FIG. 5. Present differential cross sections ($\times 10^{-20}$ m^2/sr) for electron impact excitation of the Band IV electronic states in phenol. Current measured data (•) are shown, as are the earlier benzene data for excitation of the $^1E_{1u}$ electronic-state from Kato *et al.*[17] (■).

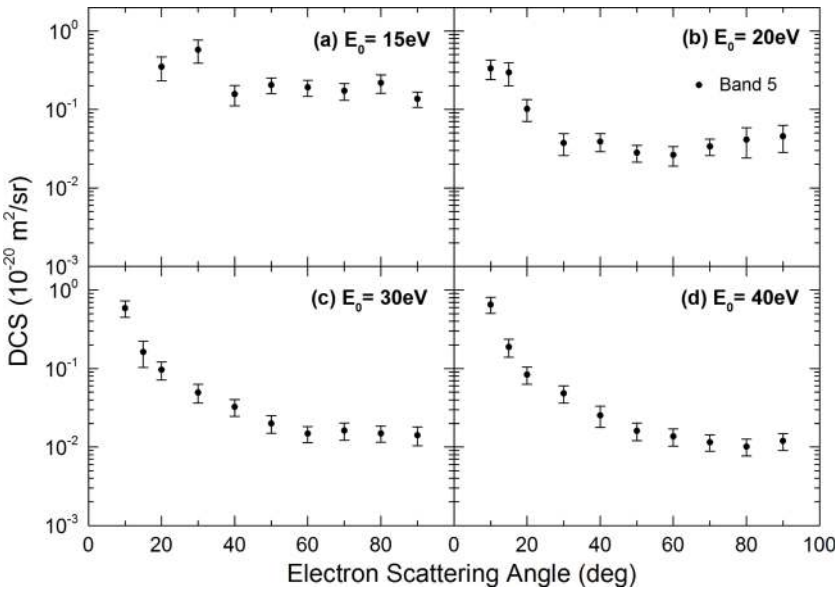

FIG. 6. Present differential cross sections ($\times 10^{-20}$ m^2/sr) for electron impact excitation of the Rydberg band of electronic states in phenol (Band V). Current measured data (•) are shown.

and exiting in partial waves up to $L_{max} = 2$; similarly L2LL denotes an electron entering and exiting in partial waves up to $L_{max} = 2$; L4LL is the same as L2LL but with $L_{max} = 4$ and finally L10KL is the same as L2KL except now $L_{max} = 10$. In our earlier study on elastic electron scattering and the total cross sections for phenol,[4] it was quite clear that best agreement between theory and measurement was found when employing $L_{max} = 10$. We would, therefore, also expect this to be the case again here. However, it is immediately apparent from Fig. 2 that, in fact, agreement between the measured data and our theory results with $L_{max} = 10$ is, at each energy, quite poor in terms of the magnitude of the DCSs although the shape accord is quite good. Indeed of the four theoretical results that we present, the level of accord for the $L_{max} = 10$ case is in fact the worst of them all. Nonetheless, this apparent paradox can be understood as follows. For the incident electron energies of 15–40 eV, all the phenol electronic states are in fact open (see Fig. 1), whereas in our MOBSCI implementation, only a sub-set of those open channels is explicitly included in the target description. As flux must be conserved in the scattering process, the intensity that should go into Bands IV and V, and some of the states of Band III that are not included in our MOBSCI, is redistributed to those channels that are actually available in the calculation. The effect of this is to "artificially" increase the magnitude of the theoretical DCS for, in particular, Bands I–III. This is why in Fig. 2 that our "best" SMCPP-SEP calculation, i.e., for $L_{max} = 10$, overestimates the magnitude of the experimental DCSs at each energy. To investigate this "flux competition" further, we conducted additional Band I theory computations in each case for an incoming plane wave and spherical waves up to $L_{max} = 10$. At 15 eV and 20 eV, the SMCPP-SEP results were computed for 3 channels, 8 channels, 13 channels, and 23 channels in the basis, while at 30 eV and 40 eV, the theory results were now calculated for 3 channels, 8 channels, 13 channels, 23 channels, and 33 channels. While a plot of those results is not explicitly given, it is quite clear that as more channels are included into the converged SMCPP-SEP calculations, the magnitude of the theory DCS drops (at 40 eV by a factor of ~10) and trends towards the experimental results. Unfortunately, at this time, our computational resources are limited to 23 channels at 15 eV and 20 eV and 33 channels at 30 eV and 40 eV, but we believe this trend towards the measured data is clearly established. The behaviour embodied in those results is an excellent example for the important role played by multichannel coupling effects, in particular for describing electronic-state excitation in molecules by electron impact. The present results for phenol are also entirely consistent with those obtained in a recent study for the $X^1A_g \rightarrow \tilde{a}^3B_{1u}$ excitation process in C_2H_4, where multichannel coupling was also demonstrated to be important.[35] Our Band I experimental results are listed in Table I.

The interpretation of our results for Band II (see Table II and Fig. 3) is a little bit more problematic, as from Jones *et al.*,[2] it contains three triplet states and two singlet states with one of those singlet states having a quite appreciable optical oscillator strength (OOS).[2] In principle, however, both the singlet states represent dipole allowed transitions and as phenol has a permanent dipole moment of non-trivial magnitude, we also invoke Born-closure (see Sec. III) in our calculations in order to better describe their excitation process. It is clear from Fig. 3 that at each energy studied, all the experimental angular distributions are strongly peaked in magnitude as you go to the more forward scattered electron angles. It is also apparent that the degree of forward peaking increases as the incident electron energy increases. This behaviour for polar molecules with significant dipole polarisabilities has been observed by us many times previously[9–13,15,36–38] and is a signature for the important role played in the scattering dynamics by those physico-chemical properties in dipole allowed excitations. The experimental DCSs are, in most cases, qualitatively reproduced by our theory results, although once again (see the above discussion for Band I) the more precise calculation with $L_{max} = 10$ significantly overestimates the magnitude of the cross sections (in particular for $\theta \geqslant 20°$). It is important to note that the apparent agreement between the measured data and the SMCPP-SEP results, with spherical waves for the incoming

and outgoing waves up to $L_{max} = 2$, is almost certainly fortuitous. In our previous study of the elastic and total cross sections for electron–phenol scattering,[4] that level of computation gave results that were significantly lower in magnitude than the experimental data. Hence it cannot be relied upon to provide a realistic description for electronic-state excitations for either the singlet or triplet states. The role of "flux competition" was also investigated for the Band II states where we undertook additional SMCPP-SEP calculations, also in each case for an incoming plane wave and outgoing spherical waves up to $L_{max} = 10$. Similar to the case for Band I, at 15 eV and 20 eV, those theory results were performed for 3 channels, 8 channels, 13 channels, and 23 channels, while at 30 eV and 40 eV, they were now done for 3, 8, 13, 23, and 33 channels. The important role played by multichannel coupling effects is also apparent for Band II, where as more "channels" are incorporated into the open channel space, the DCS magnitude is seen to decrease and trend towards the measured data. Note that this observation for Band II, as well as that made previously for Band I, is entirely consistent with that given in our earlier elastic scattering study.[4]

In Table III, we list the present measured DCS for excitation of the phenol Band III electronic-states, while in Fig. 4, those data and our 23 channel and 33 channel SMCPP-SEP results, at various levels of complexity, are plotted. Band III consists of four singlet ($^1A''$ and $^1A'$ symmetry) and four triplet ($^3A''$ symmetry) electronic-states, with the strongest dipole-allowed transitions being due to a $\pi\pi^*$ transition associated with the ring.[2] Note that for this band, the experimental measurement "captures" all eight of the excited electronic states, while our theory results only include five of the eight states due to computational limitations associated with the size of the basis that can be handled in the scattering code. Therefore in this case, a direct comparison between our measured and computed DCSs will probably be somewhat limited. Nonetheless, we note that all the Band III dipole-allowed singlet → singlet excitations that we incorporate in our basis also allow for Born-closure. Similar to what we have just described for Band II, although with the possible partial exception of the 15 eV experimental data, the present measured DCSs are again found to be peaked in magnitude at more forward scattered electron angles, with this degree of forward peaking increasing as the impact energy increases from 15 eV to 40 eV (see Fig. 4). Therefore, the role of the dipole moment and dipole polarisability of the target species on the collisional dynamics is again seen here. Also included in Fig. 4, at 15 eV and 30 eV, are DCSs for excitation of the unresolved $^1B_{1u}$ and $^3E_{2g}$ electronic states of benzene from Kato *et al.*[17] The $^1B_{1u}$ excitation process can also be associated with a weak $\pi\pi^*$ transition of the ring and thus to some extent can be thought of as corresponding to the optically allowed $^1A'$ transition in phenol. In both benzene and phenol, this transition couples to the vibrational motion to gain significant intensity, with observed optical oscillator strengths of 0.090 and 0.10–0.13 of the $^1B_{1u}$ electronic-state of benzene and the dominant $^1A'$ state of phenol, respectively. The results at 15 eV, comparing the phenol Band III DCSs to the ($^1B_{1u} + {}^3E_{2g}$) benzene DCSs, are what one might have anticipated with the magnitude of the phenol cross section being stronger than that of the benzene data across the common scattered electron angular range. This follows because at 15 eV, the triplet contributions might be anticipated to be relatively significant, as triplet excitations in general become stronger in magnitude closer to their threshold energies, and there are 4 triplet states in Band III of phenol vis-à-vis 1 doubly degenerate triplet state for benzene. Similarly, there are 3 optically active singlet Band III phenol states compared to just the $^1B_{1u}$ state in benzene. However, in this case, the "density of states" argument is not expected to play a significant role as the optical intensities for the bands are comparable. This is particularly evident from Fig. 4 at 30 eV. Here the behaviour at 30 eV, where the phenol and benzene DCSs are, to within the stated uncertainties on each measurement, very similar. One possible rationale to explain that observation is that by 30 eV the triplet contributions, in both phenol and benzene, are relatively small so that the scattering behaviour is mainly governed by excitation of the singlet states. Further, at 30 eV, the benzene cross section is somewhat larger than that observed for phenol. We have observed a similar phenomenon previously when excitation processes of benzene were compared to those in pyrimidine,[10] which has a similar 6-atom ring structure. In that study, it was postulated that the origin of this effect may reflect some orientation dependence in the electron scattering behaviour. Likewise, in this case, the attachment of the hydroxyl group to the ring destroys the high-symmetry in benzene and may alter the incoming and outgoing electron scattering conditions. In this respect, DCSs for excitation processes in oriented molecules are highly desirable to shed light onto this issue.

While Band IV (see Fig. 1) contains 21 excited electronic states, being comprised of 10 singlet states of $^1A'$ and $^1A''$ symmetry and 11 triplet states of $^3A'$ and $^3A''$ symmetry,[2] the dominant excitation process, certainly at the larger energies, is expected to be due to two experimentally unresolved $^1A'$ states with a combined optical oscillator strength of ~0.96. This is very similar to the OOS for the corresponding $^1E_{1u}$ state in benzene, which Kato *et al.*[17] determined had an OOS ~0.90. It is of further interest to note that those processes can both be considered as $\pi\pi^*$ transitions associated with the ring in each species. In Fig. 5, we therefore plot the present Band IV excitation cross sections, at 15 eV, 20 eV, 30 eV, and 40 eV, with a listing of those data being found in Table IV. It should be immediately clear from Fig. 5 that there are no other experimental or theoretical results against which we can compare the Band IV phenol data. Similar to Bands II and III, the Band IV DCS are all strongly peaked in magnitude at the more forward scattered electron angles, with the degree of this forward peaking increasing as the incident electron energy increases. We reiterate that our past experience[9–13,15,36–38] suggests that this behaviour, at least in part, reflects the important role played by the target physico-chemical properties associated with phenol's dipole moment and dipole polarisability on the collision process. We can, however, again at 15 eV and 30 eV, compare our Band IV DCSs with those for the $^1E_{1u}$ state of benzene. If we first consider 30 eV, where the triplet contributions in phenol to this band might reasonably be thought to be relatively small, we would expect the dominant dipole-allowed states in each species to largely determine the behaviour of their DCSs. Further, as the unresolved $^1A'$ states

and the $^1E_{1u}$ state have very similar OOSs, we might presuppose that both DCSs would exhibit some similarities. This is precisely what we find in Fig. 5 at the 30 eV impact energy. Again, we note that this feature may exhibit some orientation dependence in the cross section, with the benzene data similarly being slightly larger in magnitude than that for phenol (as in Band III). At 15 eV, the cumulative triplet contributions to the measured phenol DCSs will be more significant, so that we might *a priori* anticipate the Band IV phenol cross sections will be largely stronger in magnitude than those for the $^1E_{1u}$ electronic-state of benzene at that energy. This is indeed what we observe in Fig. 5 at 15 eV impact energy.

Finally, in Fig. 6 and Table V, we present the current DCSs for electron impact excitation of the Rydberg bands[2] (Band V) in phenol. There are again no independent theories or experimental data against which we can compare these results. At 30 eV and 40 eV (see Fig. 6), the observed angular distributions are consistent with what one might expect for dipole-allowed excitation,[36–38] however at 15 eV and 20 eV, the middle angle cross section magnitude is relatively more significant which suggests to us that there are also important triplet contributions to the Band V cross sections at those lower energies.

V. CONCLUSIONS

We have reported on differential cross section measurements for electron impact excitation of electronic-states in phenol. The incident electron energy interval covered in our investigation ranges from 15 to 40 eV while the scattered electron angular range was 10°–90°. The experimental measurements were complemented with sophisticated SMCPP-SEP calculations, carried out in different levels of approximation and for a sub-set (Bands I–III) of the electronic-states accessed in the experiments, with the level of agreement between theory and measurement typically being qualitatively quite good. However a mismatch, in terms of the absolute values of the cross sections, between them (when considering the results from the most accurate calculations) was found at each energy. Significant results from the present study included the roles of the target dipole moment and dipole polarisability in the scattering dynamics and, in order to obtain an accurate description for electronic-state excitation in phenol, the important role of multichannel coupling effects.

The present joint theoretical and experimental investigation is, to the best of our knowledge, the first one to report absolute DCSs for electronic-state excitations in phenol. Certainly, it is the most comprehensive thus far. Given that phenol plays an important role in organic and polymer chemistries and further given that it is well known that excitation of electronic-states potentially presents a pathway to neutral dissociation thereby leading to radical formation and chemistry, this lack of previous work was a surprise to us. In any event, we believe the current study contributes further to addressing this lack of electron–phenol scattering data in the literature. We now plan to derive integral cross sections from our DCS data, as it is the integral cross sections that are of most interest to modellers seeking to better understand biomass treatment by atmospheric pressure plasmas.

ACKNOWLEDGMENTS

This research was supported by the Australian and Brazilian Governmental Funding Agencies (ARC, CNPq and CAPES). D.B.J. thanks the ARC for a Discovery Early Career Researcher Award. R.F.C.N. acknowledges CNPq and Flinders University for financial assistance, while H.V.D. acknowledges CAPES and Flinders. M.J.B. thanks CNPq for his "Special Visiting Professor" award. E.M.O., R.F.C., M.T.N.V., and M.A.P.L. acknowledge financial support from FAPESP, while R.F.C., M.T.N.V., M.H.F.B., M.C.A.L., and M.A.P.L. acknowledge financial support from CNPq. K.L.N. thanks CNPq for an "Attracting Young Talent Grant" under the "Science Without Borders" program. G.G. acknowledges financial support from MINECO (FIS2012-31230) and COST (MP1002, CM1301).

[1]M. Weber, M. Weber, and M. Kleine-Boymann, in *Ullmann's Encyclopedia of Industrial Chemistry—Phenol* (Wiley, 2004).
[2]D. B. Jones, G. B. da Silva, R. F. C. Neves, H. V. Duque, L. Chiari, E. M. de Oliveira, M. C. A. Lopes, R. F. da Costa, M. T. do N. Varella, M. H. F. Bettega, M. A. P. Lima, and M. J. Brunger, J. Chem. Phys **141**, 074314 (2014).
[3]G. B. da Silva, R. F. C. Neves, L. Chiari, D. B. Jones, E. Ali, D. H. Madison, C. G. Ning, K. L. Nixon, M. C. A. Lopes, and M. J. Brunger, J. Chem. Phys. **141**, 124307 (2014).
[4]R. F. da Costa, E. M. de Oliveira, M. H. F. Bettega, M. T. do N. Varella, D. B. Jones, M. J. Brunger, F. Blanco, R. Colmenares, P. Limão-Vieira, G. García, and M. A. P. Lima, J. Chem. Phys. **142**, 104304 (2015).
[5]J. Amorim, C. Oliveira, J. A. Souza-Corrêa, and M. A. Ridenti, Plasma Processes Polym. **10**, 670 (2013).
[6]E. M. de Oliveira, R. F. da Costa, S. d A. Sanchez, A. P. P. Natalense, M. H. F. Bettega, M. A. P. Lima, and M. T. do N. Varella, Phys. Chem. Chem. Phys. **15**, 1682 (2013).
[7]M. E. Himmel, S.-Y. Ding, D. K. Johnson, W. S. Adney, M. R. Nimlos, J. W. Brady, and T. D. Foust, Science **315**, 804 (2007).
[8]E. M. de Oliveira, S. d A. Sanchez, M. H. F. Bettega, A. P. P. Natalense, M. A. P. Lima, and M. T. do N. Varella, Phys. Rev. A **86**, 020701(R) (2012).
[9]T. P. T. Do, M. Leung, M. Fuss, G. Garcia, F. Blanco, K. Ratnavelu, and M. J. Brunger, J. Chem. Phys. **134**, 144302 (2011).
[10]D. B. Jones, S. M. Bellm, P. Limão-Vieira, and M. J. Brunger, Chem. Phys. Lett. **535**, 30 (2012).
[11]D. B. Jones, S. M. Bellm, F. Blanco, M. Fuss, G. García, P. Limão-Vieira, and M. J. Brunger, J. Chem. Phys. **137**, 074304 (2012).
[12]Z. Mašín, J. D. Gorfinkiel, D. B. Jones, S. M. Bellm, and M. J. Brunger, J. Chem. Phys. **136**, 144310 (2012).
[13]H. V. Duque, L. Chiari, D. B. Jones, P. A. Thorn, Z. Pettifer, G. B. da Silva, P. Limão-Vieira, D. Duflot, M.-J. Hubin-Franskin, J. Delwiche, F. Blanco, G. García, M. C. A. Lopes, K. Ratnavelu, R. D. White, and M. J. Brunger, Chem. Phys. Lett. **608**, 161 (2014).
[14]P. Limão-Vieira, D. Duflot, M.-J. Hubin-Franskin, J. Delwiche, S. V. Hoffmann, L. Chiari, D. B. Jones, M. J. Brunger, and M. C. A. Lopes, J. Phys. Chem. A **118**, 6425 (2014).
[15]L. Chiari, H. V. Duque, D. B. Jones, P. A. Thorn, Z. Pettifer, G. B. da Silva, P. Limão-Vieira, D. Duflot, M.-J. Hubin-Franskin, J. Delwiche, F. Blanco, G. García, M. C. A. Lopes, K. Ratnavelu, R. D. White, and M. J. Brunger, J. Chem. Phys. **141**, 024301 (2014).
[16]See http://cccbdb.nist.gov/ for information about phenol's average dipole polarisability.
[17]H. Kato, M. Hoshino, H. Tanaka, P. Limão-Vieira, O. Ingólfsson, L. Campbell, and M. J. Brunger, J. Chem. Phys. **134**, 134308 (2011).
[18]T. Ari, H. Güven, and N. Ecevit, J. Electron Spectrosc. Relat. Phenom. **73**, 13 (1995).
[19]K. D. Jordan, J. A. Michejda, and P. D. Burrow, J. Am. Chem. Soc. **98**, 7189 (1976).
[20]M. V. Muftakhov, R. V. Khatymov, and V. A. Mazunov, Rapid Commun. Mass Spectrom. **14**, 1468 (2000).
[21]K. Kimura and S. Nagakura, Mol. Phys. **9**, 117 (1965).
[22]M. J. Brunger and P. J. O. Teubner, Phys. Rev. A **41**, 1413 (1990).
[23]M. N. R. Ashfold, G. A. King, D. Murdock, M. G. D. Nix, T. A. A. Oliver, and A. G. Sage, Phy. Chem. Chem. Phys. **12**, 1218 (2010).

[24]O. P. J. Vieuxmaire, Z. Lan, A. L. Sobolewski, and W. Domcke, J. Chem. Phys. **129**, 224307 (2008).
[25]N. Kishimoto, M. Furuhashi, and K. Ohno, J. Electron Spectrosc. Relat. Phenom. **113**, 35 (2000).
[26]M. Allan, J. Phys. B: At., Mol. Opt. Phys. **38**, 3655 (2005).
[27]H. Cho, R. J. Gulley, K. Sunohara, M. Kitajima, L. J. Uhlmann, H. Tanaka, and S. J. Buckman, J. Phys. B: At., Mol. Opt. Phys. **34**, 1019 (2001).
[28]R. J. Gulley and S. J. Buckman, J. Phys. B: At., Mol. Opt. Phys. **32**, L405 (1999).
[29]K. Takatsuka and V. McKoy, Phys. Rev. A **24**, 2473 (1981); **30**, 1734 (1984).
[30]J. S. dos Santos, R. F. da Costa, and M. T. do N. Varella, J. Chem. Phys. **136**, 084307 (2012).
[31]M. H. F. Bettega, L. G. Ferreira, and M. A. P. Lima, Phys. Rev. A **47**, 1111 (1993).
[32]R. F. da Costa, F. J. da Paixão, and M. A. P. Lima, J. Phys. B: At., Mol. Opt. Phys. **37**, L129 (2004).
[33]Z. Mašín and J. D. Gorfinkiel, J. Chem. Phys. **137**, 204312 (2012).
[34]T. P. T. Do, K. L. Nixon, M. Fuss, G. García, F. Blanco, and M. J. Brunger, J. Chem. Phys. **136**, 184313 (2012).
[35]R. F. da Costa, M. H. F. Bettega, M. T. do N. Varella, E. M. Oliveira, and M. A. P. Lima, Phys. Rev. A **90**, 052707 (2014).
[36]P. A. Thorn, M. J. Brunger, P. J. O. Teubner, N. Diakomichalis, T. Maddern, M. A. Bolorizadeh, W. R. Newell, H. Kato, M. Hoshino, H. Tanaka, H. Cho, and Y.-K. Kim, J. Chem. Phys. **126**, 064306 (2007).
[37]M. J. Brunger, L. Campbell, D. C. Cartwright, A. G. Middleton, B. Mojarrabi, and P. J. O. Teubner, J. Phys. B: At., Mol. Opt. Phys. **33**, 783 (2000).
[38]H. Kawahara, D. Suzuki, H. Kato, M. Hoshino, H. Tanaka, O. Ingölfsson, L. Campbell, and M. J. Brunger, J. Chem. Phys. **131**, 114307 (2009).